10446 *Biochemistry* **2009,** *48,* 10446–10456
DOI: 10.1021/bi9014665

BIOCHEMISTRY
including biophysical chemistry & molecular biology
Article

The Membrane Topography of the Diphtheria Toxin T Domain Linked to the A Chain Reveals a Transient Transmembrane Hairpin and Potential Translocation Mechanisms[†]

Jie Wang and Erwin London*

Department of Biochemistry and Cell Biology, Stony Brook University, Stony Brook, New York 11794-5215

Received August 20, 2009; Revised Manuscript Received September 24, 2009

ABSTRACT: The diphtheria toxin T domain helps translocate the A chain of the toxin across membranes. To gain insight into translocation, the membrane topography of key residues in T domain attached to the A chain (AT protein) was compared to that in the isolated T domain using fluorescence techniques. This study demonstrates that residues in T domain hydrophobic helices (TH5−TH9) tended to be less exposed to aqueous solution in the AT protein than in the isolated T domain. Under conditions in which the loop connecting TH5 to TH6/7 is located stably on the cis (insertion) side of the membrane in the isolated T domain, it moves between the cis and trans sides of the membrane in the AT protein. This is indicative of the formation of a dynamic, transient transmembrane hairpin topography by TH5−TH7 in the AT protein. Since TH8 and TH9 also form a transmembrane hairpin, this means that TH5−TH9 may form a cluster of transmembrane helices. These helices have a nonpolar surface likely to face the lipid bilayer in a helix cluster and a surface rich in uncharged hydrophilic residues which in a helix cluster would likely be facing inward (and perhaps be pore-lining). This uncharged hydrophilic surface could play a crucial role in translocation, interacting transiently with the translocating A chain. A similar motif can be found in, and may be important for, other protein translocation systems.

Diphtheria toxin, one of the best known and well-studied A-B bacterial toxins, is secreted as a proenzyme composed of a single polypeptide chain having a molecular mass of 58 kDa (*1*, *2*). The toxin undergoes a two-step maturation process. In the first step, it is proteolytically nicked into two polypeptide chains: the A chain (21 kDa), which forms the N-terminal part of the toxin, and the B chain (37 kDa), which forms the C-terminal part. The two chains are joined by a single disulfide bond. The B chain is made up of the receptor-binding (R) domain and the highly helical "transmembrane" (T) domain (*3*−*5*). The R domain, which forms the C-terminal part of the B chain, contains a site that binds on the cell surface to the heparin-binding epidermal growth factor-like protein, aided by CD9 (*6*−*8*). The T domain, which forms the N-terminal half of the B chain, contains hydrophobic sequences that insert into membranes and aid the translocation of the A chain.

In the cell entry process, the receptor-bound toxin undergoes endocytosis. The T domain then undergoes low-pH-triggered insertion into endosomal membranes, and at some point, a second maturation step occurs, in which there is reduction of the A−B disulfide bond. This releases the A chain [also called the catalytic (C) domain] into the cytoplasm, where it catalyzes ADP ribosylation of the diphthamide residue of elongation factor 2. This shuts down protein synthesis and leads to cell death (*9*, *10*). The last stages of translocation, including the reduction step, may be aided by cytosolic proteins (*11*, *12*).

The detailed mechanism by which the diphtheria toxin A chain is translocated across the lipid bilayer of cell membranes remains elusive. The T domain clearly has a key role in promoting translocation. At low pH, the T domain forms a pore through which the A chain might pass, and it may also function as a chaperone, interacting with the partly unfolded translocating A chain to prevent A chain refolding during translocation (*9*, *13*−*16*).

Defining the structure of the membrane-inserted T domain is likely to provide additional insights into the mechanism of translocation. Some aspects of the conformation of the membrane-inserted T domain at low pH have been characterized. It can exist both in shallowly inserted (P state) and deeply inserted (TM state) conformations (*17*−*22*). Formation of the TM state is promoted by a high concentration of T domain in the membrane, a thin bilayer width, and interactions with molten globule conformation proteins (*13*, *17*−*20*). Both the P and TM conformations are pretranslocation states, with the A chain and N-terminal segments of the T domain located on the cis side of the bilayer. The T domain can also exist in a post-translocation conformation in which the A chain and N-terminal segments of the T domain have moved to the trans side of the bilayer (*23*).

In the P state, all T domain helices (TH1−TH9) lie near the membrane surface. In contrast, in the TM state T domain, hydrophobic helices (TH5−TH9) insert deeply. The TH8−TH9 region inserts in the form of a transmembrane hairpin (*18*, *23*−*25*), connected by a short loop (TL5) containing acidic residues whose protonation at low pH has been proposed to aid membrane insertion (*18*, *24*, *26*). TH8 and TH9 are critical for, and at least under some conditions sufficient for, pore formation (*25*, *27*−*29*). The structure and functional role of hydrophobic helices TH5−TH7 is less clear. They form two hydrophobic segments, TH5 and TH6/7. TH5 has been previously reported to insert into membranes (*23*, *30*). Like TH8 and

[†]This work was supported by National Institutes of Health Grant GM 31986.

*To whom correspondence should be addressed. Telephone: (631) 632-8564. Fax: (621) 632-8575. E-mail: erwin.london@stonybrook.edu.

 Published on Web 09/25/2009

TH9, TH5−TH7 insert shallowly in the P state and deeply in the TM state (*31*). However, although there was speculation that they might form a transmembrane hairpin in membranes (*24*), they do not form a transmembrane hairpin in the TM state [the name "TM state" as used here refers to the conformation in which TH8 and TH9 form a transmembrane structure], and the loop connecting TH5 to TH6/7 remains exposed on the cis side of the bilayer upon insertion (*27*, *31*). Interestingly, disruption of deep insertion of TH8 and TH9 by mutagenesis also disrupts deep insertion of TH5−TH7 (*32*), and disruption of insertion of TH5 affects insertion of TH8 and TH9 (*33*), indicating that TH8 and TH9 and TH5−TH7 interact with each other in the TM state. Disruption of TH5 insertion also reduces the level of pore formation (*33*).

The remaining T domain helices include amphiphilic helix TH1 and hydrophilic helices TH2−TH4. Protonation of His in these segments appears to play an important role in triggering low-pH-induced changes in T domain structure (*34*, *35*). TH1−TH4 shallowly insert in both the P and TM states (*36*). They may form a flexible tether to the A chain, although TH1 may play a more direct role in one or more stages of the translocation process (*37*).

The behavior of the A chain is less well understood. The isolated A chain undergoes a reversible conformational change at low pH, undergoing partial unfolding to form a molten globule-like state and gaining the ability to associate with model membranes (*15*, *38*−*41*). The A chain shallowly inserts into the membrane all along its sequence (*15*, *41*), although one study has reported possible deeply inserted segments (*40*).

Our group has found that at low pH the addition of proteins in a partly unfolded, molten globule-like conformation, including the A chain, converts the T domain from the P to TM state, suggesting A−T interactions are an important aspect of diphtheria toxin membrane insertion (*13*). To investigate how the interaction between the A chain and T domain alters their behavior and leads to translocation in this report, we compare the topography of the isolated T domain to that when it is covalently associated as in the intact toxin (AT protein). The results show that the covalently attached A chain alters T domain topography, with TH5 and TH6/7 apparently forming a transient transmembrane hairpin that may play an important role in translocation. The results identify a possible translocation-aiding motif that may be conserved in other systems that translocate unfolded proteins across membranes.

EXPERIMENTAL PROCEDURES

Materials. 1,2-Dioleoyl-*sn*-glycero-3-phosphocholine (DOPC), 1,2-dimyristoleoyl-*sn*-glycero-3-phosphocholine (DMoPC), and 1,2-dioleoyl-*sn*-glycero-3-phosphoglycerol (DOPG) were purchased from Avanti Polar Lipids (Alabaster, AL). Lipid concentrations were determined by dry weight. *N*-[(4,4-Difluoro-5,7-dimethyl-4-bora-3a,4a-diaza-*s*-indecene-3-yl)methyl]iodoacetamide (BODIPY-FL C1-IA, BODIPY-IA), monochlorobimane, Lissamine rhodamine B-1,2-dihexadecanoyl-*sn*-glycero-3-phosphoethanolamine triethylammonium salt (Rho-DHPE), and rabbit anti-BODIPY-FL IgG were purchased from Invitrogen (Molecular Probes, Eugene, OR). *Pfx* polymerase, restriction enzymes *Eco*RI and *Nde*I, synthetic oligonucleotides, alkaline phosphatase, and T4 ligase were purchased from Invitrogen (Rockville, MD). Human serum albumin (HSA) was obtained from Worthington Biochemical (Lakewood, NJ). D-Biotin was purchased from Sigma-Aldrich. BODIPY−streptavidin conjugate (BOD−SA) (discontinued except as a custom labeling product), streptavidin (SA), and *N*-(biotinoyl)-*N*′-(iodoacetyl)-ethylenediamine (biotin-IA) were purchased from Molecular Probes. Endoproteinase Arg C was from Roche Diagnostics Corp. (Indianapolis, IN). All other chemicals were reagent grade.

Site-Directed Mutagenesis. The DNA encoding the AT protein contained diphtheria toxin residues 1−382 cloned into the pET-28a plasmid and containing the E148S substitution, which abolishes toxicity (*42*), and a N-terminal His tag used for protein purification (*36*). Next, the native Cys residues at positions 186 and 201 were replaced with Ser by mutagenesis to prepare a Cys-less template, and the nicking site (Arg^{190}-Val-Arg-Arg^{193}) in the loop between the A and T domains was mutated to a Gly-Gly-Gly-Gly sequence to abolish the sensitivity of the AT protein to degradation by proteases during isolation and storage using the procedures described previously (*33*). Two-step (asymmetric) PCR was used to introduce single-cysteine mutations into the AT protein as previously described (*31*). The mutant complementary primers, which contained the desired single-amino acid mutation, were 30−33 bp in length. PCR was conducted on an Eppendorf Mastercycler Personal PCR System using *Pfx* polymerase. The mutations were confirmed by automated DNA sequencing (Genewiz, South Plainfield, NJ). DNA sequencing also confirmed that no undesired mutations were introduced.

Expression and Purification of AT Mutants. AT proteins were overexpressed and isolated from *Escherichia coli* as described previously for the isolated T domain (*20*, *31*), except that because pET-28a was used, kanamycin (50 μg/mL) was used to select plasmid-containing bacteria (*32*, *38*). The mutant proteins were purified essentially as described previously (*20*, *27*, *31*). The first step involved affinity chromatography using a Talon metal affinity resin (CLONTECH, Palo Alto, CA). Generally, the *E. coli* extract (50 mL) was loaded onto a column containing 0.6 mL of Talon metal affinity resin followed by washing with binding buffer [5 mM imidazole, 0.5 M NaCl, and 20 mM Tris-HCl (pH 8.0)]. Most of the AT protein eluted in three 1.0 mL aliquots of elution buffer [200 mM imidazole, 0.5 M NaCl, and 20 mM Tris-HCl (pH 8.0)]. In the second step, proteins were treated with dithiothreitol (100 mM) and then subjected to FPLC with a 3 mL Source Q anion exchange column (Amersham Bioscience, Piscataway, NJ) (*27*, *31*, *38*). AT protein was eluted using a 0 to 500 mM NaCl linear gradient containing 20 mM Tris-HCl (pH 8.0) with the total volume of elution buffer being 10 mL. Elution was conducted at a rate of 0.5 mL/min, and twenty fractions (0.5 mL) were collected. AT protein generally eluted between 300 and 400 mM NaCl. The collected fractions were assessed via SDS−PAGE (8 to 25% gradient gels) using a Phastsystem (Amersham Bioscience) and Coomassie Blue staining to identify the fractions containing the protein and to determine the purity of the protein. The final purity appeared to be >95% in all cases. Protein concentrations were determined by the Bio-Rad protein assay (Bradford method) (*43*). The concentration of the isolated AT protein was generally in the range of 2−3 mg/mL. The protein was generally labeled right after purification. In some cases, the protein was stored at 4 °C, but for no more than 2 weeks. Longer storage resulted in degradation of the protein.

Fluorescence Labeling of Diphtheria Toxin Mutant Proteins. Monochlorobimane and BODIPY-IA were used to label Cys in single-Cys-containing AT mutant proteins in a manner

similar to that described previously (*17*, *20*, *31*). Briefly, monochlorobimane dissolved in ethanol (20:1 probe:AT protein molar ratio) or BODIPY-IA dissolved in dimethyl sulfoxide (8:1 probe: AT protein molar ratio) was used. All samples (1 mL containing 200−500 μg/mL protein) were labeled at room temperature for 1 h followed by overnight dialysis in 5 L of dialysis buffer. The dialysis buffer for bimane-labeled samples consisted of 100 mM NaCl and 20 mM Tris-HCl buffer (pH 8.0), while for BODIPY-labeled samples, the dialysis buffer consisted of 100 mM NaCl and 20 mM Tris-HCl buffer (pH 8.0) containing 0.75% (v/v) dimethyl sulfoxide (DMSO). Nearly full protein recovery was obtained (*17*). In parallel to the Cys-containing samples, samples of Cys-less AT protein were labeled using an identical protocol, to assay nonspecific labeling. Fluorescence measurements were used to compare the relative labeling efficiencies of mutant and Cys-less proteins. To avoid interference from nonspecific labeling of residues other than Cys, only preparations in which the labeling efficiency was at least 15−20 times greater than that of the Cys-less protein were used.

Preparation of Small Unilamellar Vesicles (*SUV*). Sonicated SUV, composed of DOPC and DOPG (7:3 molar ratio) or DMoPC and DOPG (7:3 molar ratio), were prepared in a manner similar to that described previously (*20*, *31*). Briefly, lipid mixtures dissolved in chloroform were dried under nitrogen for 15 min and then under high vacuum for 1 h. The dried lipids were resuspended with 0.5−1 mL in 167 mM acetate, 6.7 mM Tris-HCl, and 150 mM NaCl buffer (pH 4.3) (low-pH buffer) such that the total lipid concentration was 10 mM, and then the samples were sonicated to near clarity using a bath sonicator (Special Ultrasonic Cleaner Model G112SP1 Laboratory Supplies Co., Hicksville NY). The SUV preparations were stored at 4 °C for no more than 3 days before they were used.

Fluorescence Measurements. Fluorescence was measured on a Spex Tau-2 Fluorolog spectrofluorimeter operating in steady state ratio mode using a semimicro quartz cuvette (excitation path length of 10 mm, emission path length of 4 mm). The excitation and emission slits were set to 4.0 mm (7.2 nm bandwidth) and 5.5 mm (9.9 nm bandwidth), respectively. Tryptophan was excited at 280 nm, and emission was measured from 300 to 400 nm at a rate of 1 nm/s. Intensities at 335 nm are reported. Bimane was excited at 375 nm, and emission spectra were recorded from 420 to 520 nm at a rate of 1 nm/s. BODIPY fluorescence was measured for 10 s with an excitation wavelength of 485 nm and an emission wavelength of 515 nm. Rhodamine fluorescence was measured for 3 s with an excitation wavelength of 565 nm and an emission wavelength of 585 nm. In all cases, background intensities from samples lacking protein were subtracted from the intensities measured in protein-containing samples. All measurements were taken at room temperature unless otherwise noted. Samples were prepared in low-pH buffer or 20 mM Tris-HCl and 150 mM NaCl (pH 8), unless otherwise noted.

Bimane Fluorescence of Vesicle-Incorporated AT Protein. Bimane-labeled AT protein was added into SUV containing 200 μM lipid dispersed in 800 μL of low-pH buffer. Typically, the final concentration of bimane-labeled AT protein was 4 μg/mL. In some samples, additional unlabeled Cys-less AT protein or human serum albumin (HSA) was then added. To do this, either an aliquot (usually 4−10 μL) of purified Cys-less AT protein (dissolved in elution buffer from FPLC) was added to yield a final unlabeled AT concentration of approximately 16 μg/mL (in an 800 μL sample) or 4 μL of 1 mg/mL HSA dissolved in water was added to give a final HSA concentration of 5 μg/mL. After the last protein was added, the samples were incubated for 30 min at room temperature and then bimane fluorescence was measured.

Quenching of BODIPY Fluorescence of Vesicle-Incorporated AT Protein by an Anti-BODIPY Antibody. Anti-BODIPY antibody binding experiments were performed in a manner similar to that described previously (*20*, *31*). BODIPY-labeled AT proteins were incubated with SUV containing 200 μM lipid in 800 μL of low-pH buffer for 30 min. Typically, the final concentration of BODIPY-labeled AT protein was 2 μg/mL. BODIPY fluorescence was measured, and then a 20 μL aliquot of anti-BODIPY antibodies [from a 3 mg/mL stock solution dissolved in phosphate-buffered saline (pH 7.2) with 5 mM azide] was added and mixed. The fluorescence intensity was remeasured after a 30 min incubation at room temperature. Samples in which additional unlabeled AT protein (Cys-less AT protein, 16 μg/mL) or HSA (5 μg/mL) had been added were prepared as described above. For each sample, four fluorescence measurements were taken both before and after addition of the antibody, mixing samples between measurements. The reported values are the average.

Preparation of Large Unilamellar Vesicles (*LUV*) *with or without Trapped Streptavidin*. Vesicles containing trapped BODIPY−streptavidin conjugate (BOD−SA), trapped unlabeled streptavidin (SA), or no trapped protein were prepared in a manner similar to that described previously (*27*, *36*). A mixture containing 10 mM lipid composed of 70 mol % DOPC, 30 mol % DOPG, 0.002 mol % Rho-DHPE (a fluorescent lipid marker), 100 μg/mL BOD−SA or SA, and 20 mg/mL *n*-octyl β-glucoside was dissolved in 150 mM acetate and 150 mM NaCl (pH 4.5) (acetate buffer) (*27*, *36*). The sample volume was 0.5 mL. After *n*-octyl β-glucoside had been removed by dialysis at 4 °C overnight, the samples were applied to a Sepharose CL-4B column (1 cm in diameter, 50 cm in length) equilibrated in acetate buffer, to separate free BOD−SA or SA from LUV-entrapped BOD−SA or SA. After elution with acetate buffer (∼1 mL per fraction), fractions containing LUV (fractions 8 and 9) were collected. Fractions containing free BOD−SA (fractions 20−24) were also collected for later use for external addition to vesicles without trapped BOD−SA. The final concentrations of BOD−SA, SA, and/or lipid were determined by measurement of BODIPY, tryptophan, and Rho-DHPE fluorescence, respectively (*27*, *36*), using a known dilution of a stock solution as a standard. Typically, the final concentrations in the vesicle-containing fractions were 2.5−5 mM lipid and 5.6−8.0 μg/mL entrapped BOD−SA in samples containing BOD−SA, 2.3−5.7 mM lipid and 3.8−6.5 μg/mL entrapped SA in samples containing unlabeled SA, and 2.3−5.7 mM lipid in samples without trapped protein.

Preparation of Biotinylated Diphtheria Toxin Mutant Proteins. AT protein mutants were labeled with the cysteine-specific biotin-IA dissolved in dimethyl sulfoxide as described previously (*27*, *36*). Generally, 2.5−3.0 mg of AT protein dissolved in 0.5 mL of elution buffer was incubated with 45−55 μL of 8 mM biotin-IA for 1 h at room temperature. To remove the excess unbound probe, the sample was placed in dialysis tubing with a molecular weight cutoff of 8000 (Spectra/Por) and then dialyzed overnight (one buffer change around 6 h) against 5 L of 10 mM Tris-HCl and 150 mM NaCl (pH 8.2) at 4 °C. The biotinylated protein was separated from unbiotinylated protein using a monomeric avidin column (Pierce Biotechnology) in a manner similar to that described previously (*27*). Samples

were loaded onto a 2.5 mL column (1 cm in diameter, 1.3 cm in length) and eluted with six separate 0.6 mL aliquots of 0.1 M phosphate, 0.15 M NaCl, and 2 mM biotin (pH 7.0) (biotin elution buffer). The fractions were subjected to SDS−PAGE (8 to 25% gradient) using the Phastsystem. The two or three fractions with the highest concentration of the biotinylated protein were combined and dialyzed against 5 L of 10 mM Tris-HCl and 150 mM NaCl (pH 8.2) at 4 °C with three buffer changes to remove the free biotin. The final protein concentration (0.1−0.5 mg/mL) was determined using the Bradford colorimetric assay (Bio-Rad, Hercules, CA) (*43*).

Interaction of Biotinylated Diphtheria Toxin Mutants with Externally Added and Vesicle-Trapped BOD−SA. The reactivity of membrane-inserted AT protein and T domain with BOD−SA was then measured in a manner similar to that described previously (*27*, *36*). Reactivity was measured under three different conditions: (1) with externally added BOD−SA ($BOD-SA_{ex}$ samples), (2) with externally added BOD−SA and trapped unlabeled SA ($BOD-SA_{ex}/SA_{tr}$ samples), and (3) with trapped BOD−SA ($BOD-SA_{tr}$ samples).

For $BOD-SA_{tr}$ samples, LUV containing trapped BOD−SA were diluted to just under 700 μL with low-pH buffer to give an entrapped BOD−SA concentration of 0.2 μg/mL. After dilution, the lipid concentration, which varied because trapping efficiency was variable, was in the range of 100−200 μM. The initial BODIPY fluorescence was measured, and then a small aliquot (1−5 μL) of concentrated AT protein was added to give a final biotinylated AT protein concentration of 0.4 μg/mL with 3.6 μg/mL unbiotinylated Cys-less AT protein in a total volume of 700 μL. After incubation for 30 min, BODIPY fluorescence was then remeasured.

For the $BOD-SA_{ex}$ and $BOD-SA_{ex}/SA_{tr}$ samples, BODIPY fluorescence was first measured in a 630 μL sample containing BOD−SA diluted to 0.22 μg/mL with low-pH buffer.

Then 70 μL of a concentrated AT protein/LUV mixture was added. This mixture contained 40 μg/mL AT protein (4 μg/mL biotinylated and 36 μg/mL unbiotinylated Cys-less AT protein) preincubated for 15 or 50 min at room temperature with LUV (with or without trapped unlabeled streptavidin). After addition to the BOD−SA-containing solution, these samples had the same final AT protein and lipid concentrations as in samples with trapped BOD−SA. Fluorescence was remeasured after a final incubation of 30 min. For the T domain, the same protocol was used (with 10% of the protein being biotinylated) except that the final concentration of T domain was 2 μg/mL.

For experiments in which the samples with trapped unlabeled SA were preincubated with AT protein or T domain for 15 min, each experiment involved duplicate samples and was repeated 3−14 (n) separate times (AT residue 1, $n = 5$; residue 163, $n = 4$; residue 186, $n = 5$; residue 203, $n = 8$; residue 211, $n = 3$; residue 293, $n = 14$; residue 324, $n = 10$; residue 378, $n = 8$; and for residue 293 in the isolated T domain, $n = 4$).

For experiments in which the samples with trapped unlabeled SA were preincubated with AT protein for 50 min, each experiment involved duplicate samples and was repeated at least 2−7 (n) times (AT residue 203, $n = 2$; residue 288, $n = 7$; residue 293, $n = 3$; residue 297, $n = 3$; and residue 324, $n = 2$).

To evaluate the percent exposure of the biotinylated residues on the outside surface of the vesicles, the percent external reactivity was calculated. For experiments in which the reactivity of the AT protein bound to empty vesicles with externally added BOD−SA ($BOD-SA_{ex}$) was compared to the reactivity of vesicle-bound AT protein with BOD−SA trapped within the vesicles ($BOD-SA_{tr}$), the percent external reactivity was calculated from the equation percent external activity (without trapped unlabeled SA) = $\{(F - F_o)_{ex}/[(F - F_o)_{ex} + (F - F_o)_{tr}]\} \times 100\%$, where ex refers to samples with external BOD−SA, tr refers to samples with trapped BOD−SA, F_o is the BOD−SA fluorescence intensity prior to the addition of AT protein [corrected for dilution when necessary (see below)], and F is the BOD−SA fluorescence intensity 30 min after incubation of AT protein with the BOD−SA-containing sample.

For experiments in which the reactivity of AT protein bound to vesicles containing trapped unlabeled SA with externally added BOD−SA ($BOD-SA_{ex}/SA_{tr}$) was compared to the reactivity of vesicle-bound AT protein with BOD−SA trapped within the vesicles ($BOD-SA_{tr}$), the percent external reactivity was calculated from the equation percent external activity (with trapped unlabeled SA) = $\{(F - F_o)_{ex\text{-}SA}/[(F - F_o)_{ex} + (F - F_o)_{tr}]\} \times 100\%$, where ex-SA refers to samples containing trapped unlabeled SA and externally added BOD−SA. For samples with externally added BOD−SA, initial BODIPY fluorescence values were corrected to what they would be after dilution by the vesicle-containing aliquot in the absence of reaction with biotinylated AT protein. Notice that the denominator in the case of samples with trapped unlabeled SA is the same as for the samples without trapped unlabeled SA; i.e., the denominator always contains the value for the sample with external BOD−SA lacking trapped unlabeled SA.

RESULTS

Residues and Methods Used To Probe AT Protein Topography. We studied AT protein, which contains the covalently linked A chain and T domain portions of diphtheria toxin [i.e., equivalent to diphtheria toxin lacking the receptor-binding domain, which can be deleted or replaced with retention of activity and membrane translocation (*44*−*46*)]. As observed in the isolated A chain, isolated T domain, and intact toxin (*15*, *38*, *47*, *48*), the AT protein undergoes a low-pH-induced conformational transition near pH 5 in which buried Trp residues become exposed and in which it becomes hydrophobic and spontaneously inserts into model membrane vesicles (Figures S1−S3 of the Supporting Information). Also, like the intact toxin and isolated T domain (*49*, *50*), the membrane-inserted AT protein forms pores at low pH (Figure S4 of the Supporting Information).

To determine how the covalent attachment of the A chain and T domain affects their membrane topography, labeling of single Cys residues was employed. Residues previously labeled in the isolated T domain were chosen for labeling in the AT protein, specifically studying residues within and around T domain hydrophobic helices TH5−TH9 (residues 276, 288, 293, 297, 311, 324, 356, and 378). Previous studies of the isolated T domain have shown that when these residues are mutated to Cys and labeled, the T domain maintains its native conformation at neutral pH and undergoes the same low-pH-induced conformational changes and lipid binding seen in the wild-type, unlabeled protein (*20*, *31*, *36*, *38*).

Two assays previously used to define the topography of the isolated T domain were used to investigate AT protein topography (*17*, *20*, *31*, *36*, *38*). First, the fluorescence emission λ_{max} of bimane-labeled residues was used to evaluate the location of labeled Cys residues. We have previously shown that bimane fluorescence blue shifts upon insertion into the lipid bilayer,

Table 1: Comparison of Bimane Emission Maximum (λ_{max}) of Bimane-Labeled Mutants in the Hydrophobic TH5−TH9 Region of the Membrane-Inserted T Domain or AT Protein at pH 4.3 and Room Temperature

		bimane emission maximum (λ_{max}) (nm)[a]					
		isolated T domain[b]		AT protein		T domain from Arg C-digested AT protein[c]	
location	residue number	DOPC/DOPG	DMoPC/DOPG	DOPC/DOPG	DMoPC/DOPG	DOPC/DOPG	DMoPC/DOPG
TH5	276	468	461	463	461	nd[d]	nd[d]
	288	472	468	465	464	470	467
TH5−TH6 loop	293	459	470	462	466	459	472
TH6/7	311	467	462	460	460	467	463
TH9	356	469	461	462	458	468	460
average without residue 293		469	463	463	461	–	–

[a]The average value from duplicate samples is shown. λ_{max} values were generally reproducible to ±1 nm. [b]Isolated T domain data from previous studies (*20*, *31*). [c]Samples containing T domain fragment from digested AT mutants using Arg C. [d]Not determined.

Table 2: Comparison of the Quenching Percentage of BODIPY Fluorescence in the TH5−TH9 Hydrophobic Region of the Model Membrane-Inserted T Domain or AT Protein by the Anti-BODIPY Antibody at pH 4.3 and Room Temperature

		% quenching of BODIPY fluorescence[a]			
		isolated T domain[b]		AT protein	
location	residue number	DOPC/DOPG	DMoPC/DOPG	DOPC/DOPG	DMoPC/DOPG
TH5	276	62.0	40.0	48.0 ± 1.9	39.0 ± 7.7
	288	25.5	33.5	37.6 ± 0.9	28.4 ± 5.0
TH5−TH6 loop	293	30.0	76.0	36.6 ± 4.6	32.6 ± 6.4
TH6/7	311	49.0	25.0	38.7 ± 1.1	12.9 ± 5.7
TH9	356	45.0	25.0	44.4 ± 4.7	26.5 ± 0.8
average without residue 293		45	31	42	27

[a]Average values from duplicate samples and their range are shown. [b]Isolated T domain data from previous studies (*20*, *31*).

and that the extent of the shift is closely correlated with the depth of insertion. Second, accessibility of BODIPY-labeled residues to the anti-BODIPY antibody was measured. This is sensitive to the burial of labeled residues within a membrane but does not measure exactly the same parameter that is measured by bimane because buried residues that are transiently exposed to aqueous solution (i.e., are not stably buried) can react with the antibody.

These methods were used to explore the conformation and topography of the AT protein when AT protein was membrane-inserted at low pH. The experiments with the membrane-inserted protein were conducted using SUV under conditions previously shown (*13*, *17*) to promote formation of the surface (P state) T domain conformation (i.e., in DOPC/DOPG vesicles), and under three different conditions that promote formation of the transmembrane (TM state) T domain conformation [i.e., (1) in DMoPC [di C14:1 PC]/DOPG vesicles, which form thinner bilayers than vesicles with DOPC [di C18:1 PC], (2) in DOPC/DOPG vesicles with a high concentration of AT protein, or (3) in DOPC/DOPG vesicles in the presence of human serum albumin, a molten globule state protein]. Although we mainly show data here only for the first set of conditions promoting formation of TM insertion, similar behavior was observed under all the different conditions that promote formation of the TM state (data not shown).

Topography of Hydrophobic Helices TH5−TH9 in the Membrane-Inserted AT Protein. The membrane topography of residues within T domain hydrophobic segments (TH5−TH9) of the AT protein was compared to that previously observed in the isolated T domain (*20*, *27*, *31*). Residues 276 and 288 (in TH5), 311 (in the TH6/7 segment), and 356 (in the middle of TH9) were chosen for study because they are within hydrophobic helices and their level of exposure to solution decreases when the T domain switches from the shallowly inserted P state to deeply inserted states (*17*, *20*, *31*). The behavior of residue 293 (in the hydrophilic loop between TH5 and TH6) was also studied. In the isolated T domain, residue 293 shows unusual behavior; it becomes more exposed to aqueous solution when the hydrophobic segments insert more deeply.

Tables 1 and 2 compare the behavior of these TH5−TH9 residues in the membrane-inserted AT protein to that previously defined for the membrane-inserted isolated T domain under both conditions that favor the formation of the P state and conditions that favor the formation of the TM state. A significant difference between the AT protein and isolated T domain was observed. When inserted into DOPC/DOPG vesicles, in which the isolated T domain forms the P state, bimane-labeled residues within the hydrophobic helices of the AT protein exhibited fluorescence that was much more blue-shifted than that of the isolated T domain in DOPC/DOPG vesicles (Table 1). Instead, the λ_{max} values were similar to those observed in the isolated T domain in DMoPC/DOPG vesicles, in which the isolated T domain forms the TM state.

However, as judged by quenching, the antibody accessibility of TH5−TH9 BODIPY-labeled residues in the AT protein inserted into DOPC/DOPG vesicles exhibited a level of reactivity between that of the T domain in the P state and that of the T domain in the TM state (Table 2). This suggests that, although TH5−TH9 residues in the AT protein in DOPC/DOPG vesicles form a

conformation similar to that of the isolated T domain in the TM state (as judged by bimane fluorescence), this deep insertion is not as stable as in the TM state formed by the isolated T domain (as reported by anti-BODIPY quenching). Alternate possibilities are that the BODIPY-labeled residues do not insert quite as deeply as bimane-labeled ones or that there is steric blockage of labeled T domain residues from aqueous solution due to the A chain.

Bimane fluorescence λ_{max} values for TH5−TH9 residues in the AT protein inserted into DMoPC/DOPG vesicles were very blue-shifted, indicating that the TM state had formed, and the values were similar (but not identical) to that for the isolated T domain in DMoPC/DOPG vesicles, which also forms the TM state under these conditions (Table 1). Furthermore, the antibody accessibility was low both for the AT protein and for the isolated T domain when inserted into DMoPC/DOPG bilayers, indicative of stable deep insertion in both of these cases (Table 2).

Intriguingly, in the AT protein, residue 293 in the hydrophilic loop connecting TH5 to TH6 behaved in an unexpected fashion in DMoPC/DOPG vesicles. In the isolated T domain in the TM state, bimane-labeled residue 293 is very red-shifted and when BODIPY-labeled is very antibody reactive (*31*) (Tables 1 and 2). In contrast, in the AT protein, labeled residue 293 showed somewhat more blue-shifted bimane fluorescence (Table 1) and a relatively low reactivity with the anti-BODIPY antibody (Table 2). This suggests there is an important difference between the topography of this region of the protein in the AT protein relative to that in the isolated T domain (see below).

To confirm that the differences between the topography of the isolated T domain and that of the AT protein were due to A−T interactions, rather than due to some undefined experimental difference between this study and previous ones, AT proteins labeled with bimane at residue 288, 293, 311, or 356 were subjected to Arg C digestion. Arg C is an Arg-specific protease, and the T domain has Arg residues only at positions 210 and 377, near its N- and C-termini, respectively. Therefore, a limiting Arg C digestion of AT protein results in the formation of a nearly intact T domain, while the A chain, which has several Arg residues, is digested into smaller fragments (Figure S5 of the Supporting Information). Unlike what was observed before Arg C digestion, bimane λ_{max} values for the Arg C-digested labeled AT protein were almost identical to those of the isolated T domain (Table 1). This was true both for the AT protein inserted into DOPC/DOPG vesicles and for the AT protein inserted into DMoPC/DOPG vesicles. This shows that the A−T interactions abolished by Arg C digestion altered the behavior of TH5−TH9.

Distinguishing Exposure of AT Residues on the Cis and Trans Sides of the Bilayer Using Biotinylated Residues and BOD−SA. The above-noted difference between the behavior of residue 293 in the AT protein and isolated T domain suggested that there might be an important difference between their topography in this region of the protein. To see if this difference involved whether residues were exposed on the cis side (the side from which insertion occurs) or trans side of the bilayer (the side to which translocation moves residues), the accessibility of biotinylated residues of membrane-inserted AT protein to BODIPY-labeled strepatavidin (BOD−SA) was studied. These experiments were conducted with the AT protein incorporated into large unilamellar vesicles (LUV) composed of DOPC and DOPG (*27*). In these experiments, the reactivity of biotinylated residues with BOD−SA externally added to vesicles (i.e., on the cis side of the membrane) is compared to the reactivity with

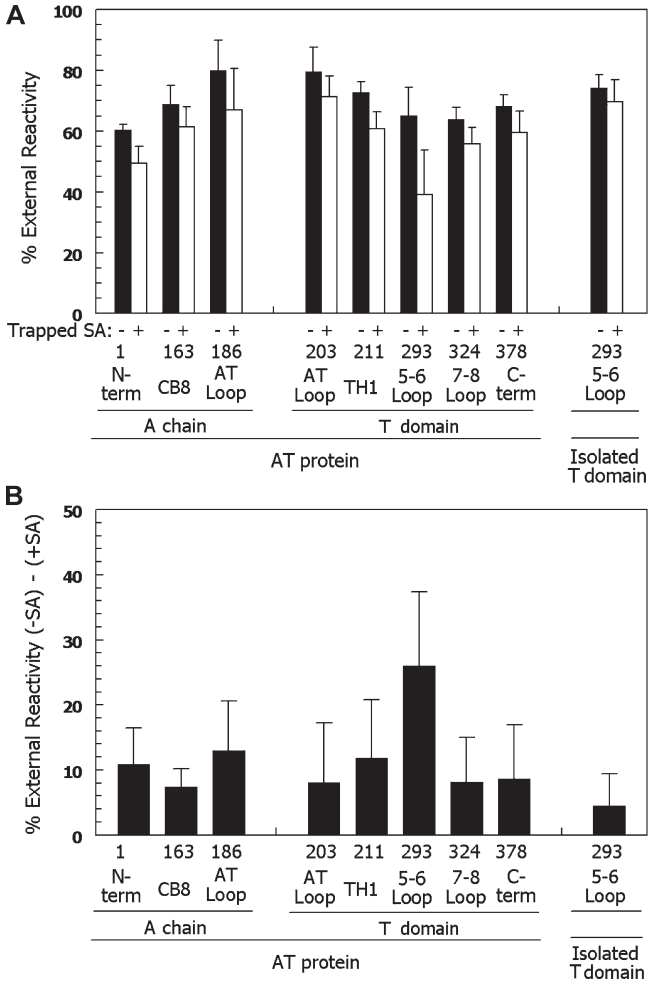

FIGURE 1: Cis−trans surface localization of biotinylated AT protein residues in membrane-inserted AT proteins by determination of percent external reactivity. (A) The percent external reactivity (reaction with external BOD−SA/total reactivity with trapped and external BOD−SA) × 100% is shown for a series of biotinylated Cys mutants. Samples containing 4 μg/mL total AT protein (0.4 μg/mL biotinylated AT protein, 3.6 μg/mL unlabeled Cys-less AT protein), 0.2 μg/mL BOD−SA, and 0.10−0.21 mM lipid (70 mol % DOPC/30 mol % DOPG LUV) in low-pH buffer (pH 4.3). Samples in which reactivity with external BOD−SA was measured were preincubated for 15 min with vesicles without (black bars) or with (white bars) 0.2 μg/mL entrapped unlabeled SA. Experiments were conducted at room temperature. In most cases, the average values from four or five experiments and standard deviations are shown. (B) Difference between percent external reactivity for experiments without and with trapped unlabeled SA. The value of the difference with and without trapped unlabeled SA was calculated first, and then the average and standard deviation of the differences were calculated. See Experimental Procedures for details. The *x*-axis shows the residue number and the segment of the protein in which it is located. The behavior of biotinylated residue 293 in the isolated T domain is also shown as a control.

BOD−SA that is vesicle-entrapped (i.e., on the trans side) (see schematic Figure 3 in ref *27*). It should be noted that biotinylation of diphtheria toxin residues does not interfere with their translocation across a bilayer (*23*, *27*), and that in these LUV, the isolated T domain forms the TM state (*27*).

Figure 1 summarizes the reactivity of a series of biotinylated residues with BOD−SA. Most residues were more reactive with externally added BOD−SA than vesicle-entrapped BOD−SA (black bars), such that 60−80% of each residue was exposed on the cis surface. This is in agreement with our previous studies

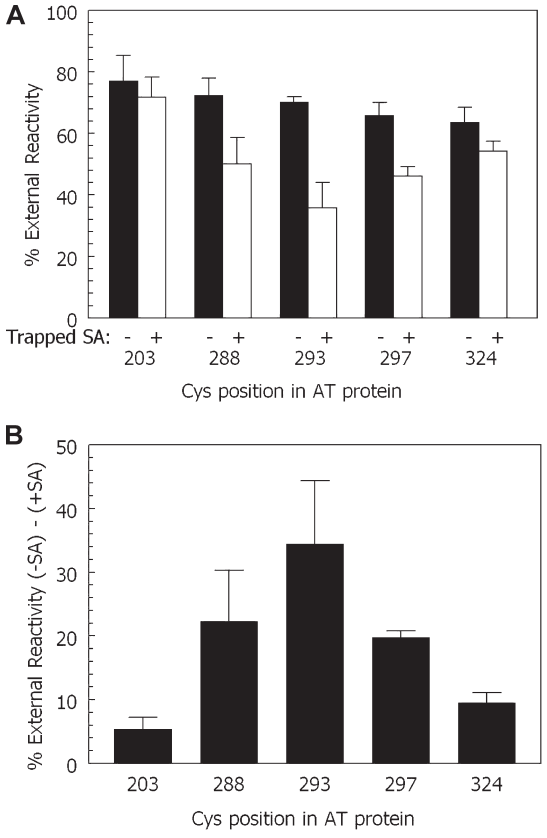

FIGURE 2: Cis−trans surface localization of biotinylated residues in and around the TH5−TH6 loop in the membrane-inserted AT protein at pH 4.3 and room temperature. (A) Percent external reactivity for residues in and around the AT loop measured under the same conditions as described in the legend of Figure 1 except that samples in which reactivity with external BOD-SA was measured were preincubated for 50 min with vesicles without (black bars) or with (white bars) 0.2 μg/mL entrapped unlabeled SA. Average values and standard deviations are shown. (B) Difference between the percent external reactivity for experiments without and with trapped unlabeled SA. The value of the difference with and without trapped unlabeled SA was calculated first, and then the average and standard deviation of the differences were calculated. The *x*-axis shows the residue number. See Experimental Procedures for details.

showing that both the whole toxin (*51*) and the isolated T domain (*27*) insert into model membranes in a mixture of orientations, and that the orientation in which most of the protein is on the cis side of the membrane predominates. The fact that residues on both the N- and C-termini of the hydrophobic TH6/7 sequence (i.e., residues 293 and 324) are predominantly exposed on the cis surface on the bilayer indicates that TH5−TH7 do not form a stable transmembrane hairpin in the AT protein and instead form a structure in which the TH5−TH6 loop (connecting TH5 to TH6/7) is exposed on the cis side of the membrane. This is in agreement with previous results with the isolated T domain (*27*).

However, this does not rule out the possibility that TH5−TH7 form a transient transmembrane hairpin in which the TH5−TH6 loop is transiently located on the trans side of the membrane. To test for this, the reactivity of AT residues with externally added BOD−SA was measured using samples containing vesicle-trapped unlabeled SA (see schematic Figure 3 in ref *27*). If residues are moving back and forth across the bilayer, which occurs when a transient transmembrane structure forms, then membrane insertion of the AT protein into vesicles containing trapped unlabeled SA should allow the biotinylated group to react with the trapped unlabeled SA and thus prevent reaction with externally added BOD−SA.

Figure 1A (white bars) shows that for almost all residues tested, including residues in the A chain and N-terminal region of the T domain, the presence of trapped unlabeled SA only slightly reduced [~10% (see Figure 1B)] the extent of the reaction of AT protein with externally added BOD−SA. This slight reduction might be due to some small amount of trapped SA that leaked out of the vesicles. In contrast, for residue 293, the presence of trapped unlabeled SA resulted in a 2.5-fold greater reduction in the extent of reaction with externally added BOD−SA (Figure 1B). This suggests that in a significant fraction of AT proteins, residue 293 is moving back and forth across the membrane.

To further confirm that the TH5−TH6 loop (which contains residue 293) was moving back and forth across the bilayer, this experiment was repeated using a longer preincubation time to amplify the reaction with trapped unlabeled SA and repeated with additional residues in and near the TH5−TH6 loop (Figure 2). Increasing the preincubation time significantly increased the level of inhibition of reactivity by trapped unlabeled SA for residue 293 (to ~35%). Under these conditions, a relatively high degree of inhibition of reactivity by trapped unlabeled SA could also be observed for residues 288 and 297. However, the inhibition was weaker than that observed with residue 293, suggesting that these residues, which are at the ends of hydrophobic helices TH5 and TH6, respectively, may not be as exposed to trapped SA as residue 293 when they face the trans side of the bilayer. It should be noted that pore formation by the AT protein cannot explain the inhibition of residue 293 reactivity in the presence of trapped unlabeled SA. The pores formed by the diphtheria toxin are too small under our experimental conditions to allow molecules as large as SA through a lipid bilayer (*50*).

As a control to confirm that the difference between the behavior of residue 293 in the AT protein and isolated T domain was reproducible, we repeated our previously published experiments using the isolated T domain (*27*). In agreement with our previous study, the reactivity of residue 293 in the isolated T domain does not exhibit the reactivity pattern (inhibition of association of biotinylated AT with BOD−SA by trapped SA) characteristic of transient translocation (Figure 1).

DISCUSSION

Comparison of TH5−TH9 Topology in the AT Protein with That in the Isolated T Domain in Model Membranes. T domain hydrophobic helices (TH5−TH9) exhibit important changes in behavior when the A chain is present. As noted above, in the membrane-inserted isolated T domain, TH5−TH9 exist in two distinct conformations, a shallowly inserted one (which forms in DOPC/DOPG SUV) and a deeply inserted one (which forms in DMoPC/DOPG SUV). As judged by bimane fluorescence and BODIPY quenching, the insertion of residues within TH5−TH9 in the AT protein in DOPC/DOPG vesicles was less exposed to solution than in the isolated T domain. This is consistent with our previous observation that noncovalent binding of the isolated A chain to the isolated T domain converts the T domain from a state in which TH5−TH9 residues are exposed to solution to one in which they are not (*13*). However, a 5-fold excess of the isolated A chain was needed to induce complete conversion of the T domain to the less solution-exposed form (*13*). Thus, the single covalently linked A chain in the

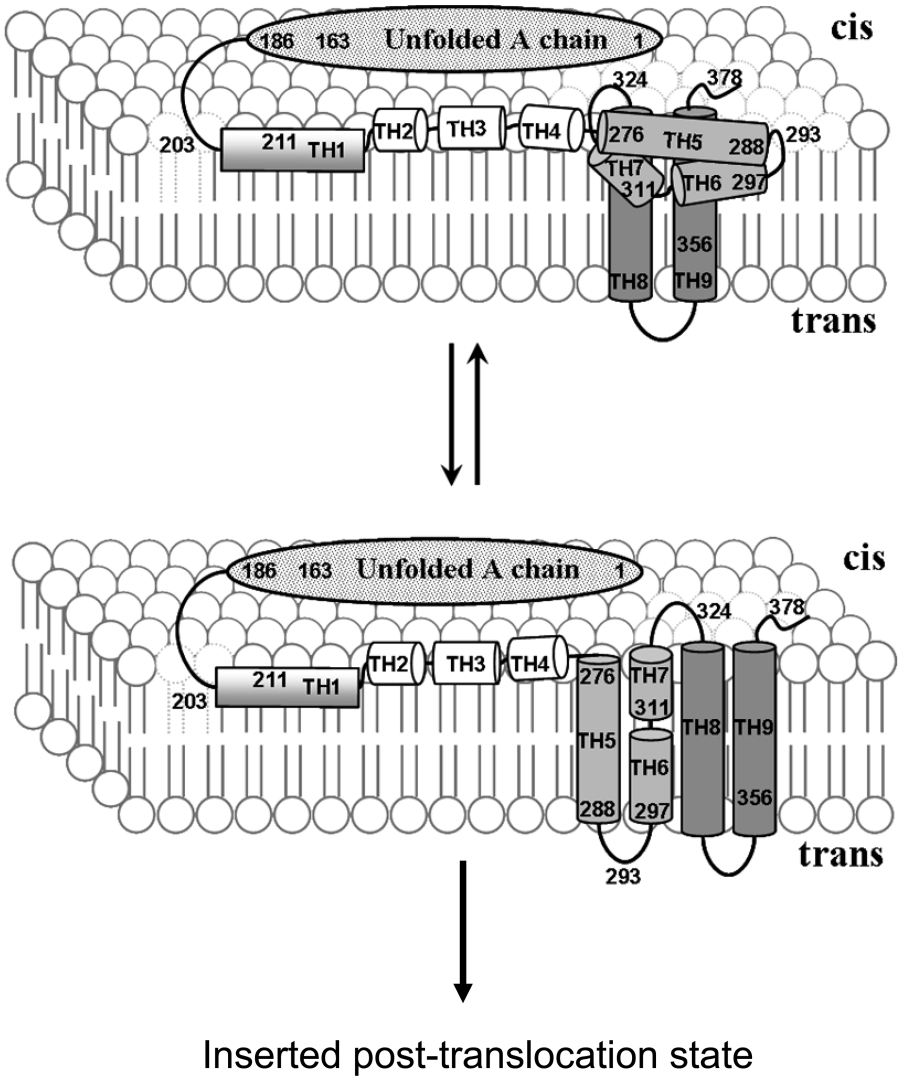

FIGURE 3: Schematic diagram showing pretranslocation states for the AT protein in model membranes at low pH. The top shows the pretranslocation TM state in which TH8 and TH9 form a transmembrane hairpin while semihydrophobic segments TH5−TH7 deeply insert without forming a transmembrane structure. The bottom shows the transient pretranslocation state in which both TH8−TH9 and TH5−TH7 form a transmembrane hairpin. This conformation might then proceed to form the previously identified post-translocation inserted state (*23*). The A chain and hydrophilic TH1−TH4 region of the T domain lie on or near the cis side surface of the bilayer in both of the pretranslocation states. The details of how the A chain interacts with the T domain and the lipid bilayer are not yet defined.

AT protein is more effective than the isolated A chain in interacting with the T domain.

The behavior of the loop connecting TH5 to TH6 was also different in the AT protein and isolated T domain. In the isolated T domain, residue 293, which is within this loop, has the unusual property of inserting shallowly when TH5−TH9 helix residues insert deeply, and deeply when TH5−TH9 helix residues insert shallowly. However, when TH5−TH9 helix residues inserted deeply into the AT protein, residue 293 appeared to insert more deeply than in the isolated T domain. This suggests a significant difference between the insertion of the TH5−TH7 helix cluster in the AT protein and isolated T domain. This difference was confirmed by the BOD−SA assay, which showed that residue 293, which remains on the cis side of the membrane in the isolated T domain (*27*), dynamically interconverts between the cis and trans sides of the membrane in a population of AT protein. It should be noted that additional studies of Cys-labeled residues in the A chain in the AT protein, and TH1 of the T domain in the AT protein, show relatively shallow insertion, as is the case in the isolated A chain and T domain (data not shown). Combined, the experimental data suggest the model for AT protein topographies shown in Figure 3. If correct, this model would support the original suggestion (*24*) that TH5−TH7 would form a transmembrane hairpin (with TH5 forming one transmembrane segment and TH6/7 forming the other), except that the transmembrane insertion of TH5−TH7 would be dynamic, rather than stable. This dynamic instability is not wholly surprising because the TH5−TH7 sequence has borderline hydrophobicity, being less hydrophobic than most transmembrane segments of ordinary membrane proteins and than the other hydrophobic diphtheria toxin helices, TH8 and TH9 (*52*).

Insights into the Mechanism of Translocation. What insights into the mechanism of translocation do the topographical properties of TH5−TH9 provide? One speculative possibility is that in a fully transmembrane state TH5−TH9 form the wall of the pathway ("pore") through which the A chain moves during translocation. In this regard, it is noteworthy that these segments have considerable amphiphilic character and would be expected to be arranged with their more polar face forming the pore/translocation pathway, as shown in Figure 4. The hydrophilic

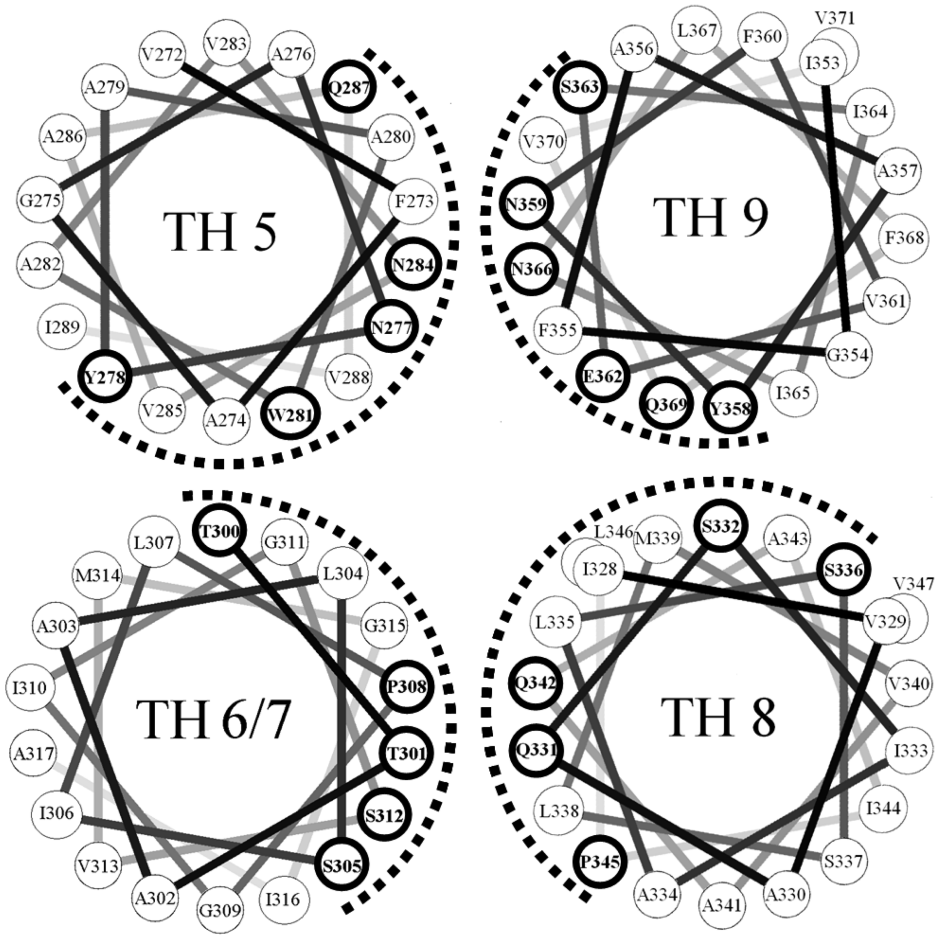

FIGURE 4: Helical wheel representation of TH5−TH9. The dashed line indicates the more polar face of the hydrophobic segments. Residues with hydrogen bonding abilities are shown in bold circles. Notice that Trp and Tyr are located near the center of hydrophobic segments, which is unusual in transmembrane helices. Helical wheel adapted from: http://rzlab.ucr.edu/scripts/wheel/wheel.cgi.

face formed by this cluster is rich in uncharged polar residues (Gln, Asn, Ser, and Thr) and has no charged residues (with the possible exception of Glu362, which might be protonated and thus uncharged at low pH). This may be significant because inspection of crystal structures shows that this type of hydrophilic/uncharged surface is seen in the pore-facing surface of other protein translocators, specifically, the Sec Y translocon (*53*) and Tol C (*54*), and may represent a common translocator wall motif. We speculate that the lack of charged amino acids prevents overly strong interactions between the T domain and translocating A chain. Transient interactions between the unfolded A chain and the hydrophilic surface of TH5−TH9 would be consistent with the chaperone model we proposed previously for A chain−T domain interactions (*13*, *14*).

The dynamic equilibration of TH5−TH7 might also play a role similar to that recently proposed for the Sec A protein, in which a hairpin segment of Sec A binds to the translocation substrate and then carries it across the membrane (*55*, *56*). If the TH5−TH6 loop binds to the A chain, as it moves back and forth across the bilayer it could shuttle the A chain across the bilayer in a series of steps, probably aided by cytosolic proteins (*11*, *12*). The binding and release of the A chain might be controlled by the pH gradient across the endosomal membrane, if binding to the A chain occurs at low pH on the cis side of the membrane while dissociation of the A chain occurs at neutral pH, which is found on the trans side of the membrane.

SUPPORTING INFORMATION AVAILABLE

Additional experimental details and results. This material is available free of charge via the Internet at http://pubs.acs.org.

REFERENCES

1. Drazin, R., Kandel, J., and Collier, R. J. (1971) Structure and activity of diphtheria toxin. II. Attack by trypsin at a specific site within the intact toxin molecule. *J. Biol. Chem. 246*, 1504–1510.
2. Gill, D. M., and Pappenheimer, A. M., Jr. (1971) Structure-activity relationships in diphtheria toxin. *J. Biol. Chem. 246*, 1492–1495.
3. Ittelson, T. R., and Gill, D. M. (1973) Diphtheria toxin: Specific competition for cell receptors. *Nature 242*, 330–332.
4. Uchida, T., Pappenheimer, A. M., Jr., and Harper, A. A. (1972) Reconstitution of diphtheria toxin from two nontoxic cross-reacting mutant proteins. *Science 175*, 901–903.
5. Uchida, T., Pappenheimer, A. M., Jr., and Harper, A. A. (1973) Diphtheria toxin and related proteins. 3. Reconstitution of hybrid "diphtheria toxin" from nontoxic mutant proteins. *J. Biol. Chem. 248*, 3851–3854.
6. Mitamura, T., Iwamoto, R., Umata, T., Yomo, T., Urabe, I., Tsuneoka, M., and Mekada, E. (1992) The 27-kD diphtheria toxin receptor-associated protein (DRAP27) from Vero cells is the monkey homologue of human CD9 antigen: Expression of DRAP27 elevates the number of diphtheria toxin receptors on toxin-sensitive cells. *J. Cell Biol. 118*, 1389–1399.
7. Naglich, J. G., Metherall, J. E., Russell, D. W., and Eidels, L. (1992) Expression cloning of a diphtheria toxin receptor: Identity with a heparin-binding EGF-like growth factor precursor. *Cell 69*, 1051–1061.
8. Cha, J. H., Brooke, J. S., Ivey, K. N., and Eidels, L. (2000) Cell surface monkey CD9 antigen is a coreceptor that increases diphtheria toxin

sensitivity and diphtheria toxin receptor affinity. *J. Biol. Chem. 275*, 6901–6907.
9. London, E. (1992) Diphtheria toxin: Membrane interaction and membrane translocation. *Biochim. Biophys. Acta 1113*, 25–51.
10. Pappenheimer, A. M., Jr. (1977) Diphtheria toxin. *Annu. Rev. Biochem. 46*, 69–94.
11. Ratts, R., Trujillo, C., Bharti, A., vanderSpek, J., Harrison, R., and Murphy, J. R. (2005) A conserved motif in transmembrane helix 1 of diphtheria toxin mediates catalytic domain delivery to the cytosol. *Proc. Natl. Acad. Sci. U.S.A. 102*, 15635–15640.
12. Ratts, R., Zeng, H., Berg, E. A., Blue, C., McComb, M. E., Costello, C. E., vanderSpek, J. C., and Murphy, J. R. (2003) The cytosolic entry of diphtheria toxin catalytic domain requires a host cell cytosolic translocation factor complex. *J. Cell Biol. 160*, 1139–1150.
13. Ren, J., Kachel, K., Kim, H., Malenbaum, S. E., Collier, R. J., and London, E. (1999) Interaction of diphtheria toxin T domain with molten globule-like proteins and its implications for translocation. *Science 284*, 955–957.
14. Hammond, K., Caputo, G. A., and London, E. (2002) Interaction of the membrane-inserted diphtheria toxin T domain with peptides and its possible implications for chaperone-like T domain behavior. *Biochemistry 41*, 3243–3253.
15. Zhao, J. M., and London, E. (1988) Conformation and model membrane interactions of diphtheria toxin fragment A. *J. Biol. Chem. 263*, 15369–15377.
16. Papini, E., Schiavo, G., Tomasi, M., Colombatti, M., Rappuoli, R., and Montecucco, C. (1987) Lipid interaction of diphtheria toxin and mutants with altered fragment B. 2. Hydrophobic photolabelling and cell intoxication. *Eur. J. Biochem. 169*, 637–644.
17. Wang, Y., Malenbaum, S. E., Kachel, K., Zhan, H., Collier, R. J., and London, E. (1997) Identification of shallow and deep membrane-penetrating forms of diphtheria toxin T domain that are regulated by protein concentration and bilayer width. *J. Biol. Chem. 272*, 25091–25098.
18. Ren, J., Sharpe, J. C., Collier, R. J., and London, E. (1999) Membrane translocation of charged residues at the tips of hydrophobic helices in the T domain of diphtheria toxin. *Biochemistry 38*, 976–984.
19. Malenbaum, S. E., Collier, R. J., and London, E. (1998) Membrane topography of the T domain of diphtheria toxin probed with single tryptophan mutants. *Biochemistry 37*, 17915–17922.
20. Kachel, K., Ren, J., Collier, R. J., and London, E. (1998) Identifying transmembrane states and defining the membrane insertion boundaries of hydrophobic helices in membrane-inserted diphtheria toxin T domain. *J. Biol. Chem. 273*, 22950–22956.
21. Kyrychenko, A., Posokhov, Y. O., Rodnin, M. V., and Ladokhin, A. S. (2009) Kinetic intermediate reveals staggered pH-dependent transitions along the membrane insertion pathway of the diphtheria toxin T-domain. *Biochemistry 48*, 7584–7594.
22. Chenal, A., Prongidi-Fix, L., Perier, A., Aisenbrey, C., Vernier, G., Lambotte, S., Fragneto, G., Bechinger, B., Gillet, D., Forge, V., and Ferrand, M. (2009) Deciphering membrane insertion of the diphtheria toxin T domain by specular neutron reflectometry and solid-state NMR spectroscopy. *J. Mol. Biol. 391*, 872–883.
23. Senzel, L., Gordon, M., Blaustein, R. O., Oh, K. J., Collier, R. J., and Finkelstein, A. (2000) Topography of diphtheria Toxin's T domain in the open channel state. *J. Gen. Physiol. 115*, 421–434.
24. Choe, S., Bennett, M. J., Fujii, G., Curmi, P. M., Kantardjieff, K. A., Collier, R. J., and Eisenberg, D. (1992) The crystal structure of diphtheria toxin. *Nature 357*, 216–222.
25. Huynh, P. D., Cui, C., Zhan, H., Oh, K. J., Collier, R. J., and Finkelstein, A. (1997) Probing the structure of the diphtheria toxin channel. Reactivity in planar lipid bilayer membranes of cysteine-substituted mutant channels with methanethiosulfonate derivatives. *J. Gen. Physiol. 110*, 229–242.
26. Kaul, P., Silverman, J., Shen, W. H., Blanke, S. R., Huynh, P. D., Finkelstein, A., and Collier, R. J. (1996) Roles of Glu 349 and Asp 352 in membrane insertion and translocation by diphtheria toxin. *Protein Sci. 5*, 687–692.
27. Rosconi, M. P., Zhao, G., and London, E. (2004) Analyzing topography of membrane-inserted diphtheria toxin T domain using BODIPY-streptavidin: At low pH, helices 8 and 9 form a transmembrane hairpin but helices 5−7 form stable nonclassical inserted segments on the cis side of the bilayer. *Biochemistry 43*, 9127–9139.
28. Mindell, J. A., Silverman, J. A., Collier, R. J., and Finkelstein, A. (1994) Structure-function relationships in diphtheria toxin channels: III. Residues which affect the cis pH dependence of channel conductance. *J. Membr. Biol. 137*, 45–57.
29. Silverman, J. A., Mindell, J. A., Zhan, H., Finkelstein, A., and Collier, R. J. (1994) Structure-function relationships in diphtheria toxin channels: I. Determining a minimal channel-forming domain. *J. Membr. Biol. 137*, 17–28.
30. D'Silva, P. R., and Lala, A. K. (2000) Organization of diphtheria toxin in membranes. A hydrophobic photolabeling study. *J. Biol. Chem. 275*, 11771–11777.
31. Rosconi, M. P., and London, E. (2002) Topography of helices 5−7 in membrane-inserted diphtheria toxin T domain: Identification and insertion boundaries of two hydrophobic sequences that do not form a stable transmembrane hairpin. *J. Biol. Chem. 277*, 16517–16527.
32. Zhao, G., and London, E. (2005) Behavior of diphtheria toxin T domain containing substitutions that block normal membrane insertion at Pro345 and Leu307: Control of deep membrane insertion and coupling between deep insertion of hydrophobic subdomains. *Biochemistry 44*, 4488–4498.
33. Lai, B., Zhao, G., and London, E. (2008) Behavior of the deeply inserted helices in diphtheria toxin T domain: Helices 5, 8, and 9 interact strongly and promote pore formation, while helices 6/7 limit pore formation. *Biochemistry 47*, 4565–4574.
34. Perier, A., Chassaing, A., Raffestin, S., Pichard, S., Masella, M., Menez, A., Forge, V., Chenal, A., and Gillet, D. (2007) Concerted protonation of key histidines triggers membrane interaction of the diphtheria toxin T domain. *J. Biol. Chem. 282*, 24239–24245.
35. Montagner, C., Perier, A., Pichard, S., Vernier, G., Menez, A., Gillet, D., Forge, V., and Chenal, A. (2007) Behavior of the N-terminal helices of the diphtheria toxin T domain during the successive steps of membrane interaction. *Biochemistry 46*, 1878–1887.
36. Wang, J., Rosconi, M. P., and London, E. (2006) Topography of the hydrophilic helices of membrane-inserted diphtheria toxin T domain: TH1-TH3 as a hydrophilic tether. *Biochemistry 45*, 8124–8134.
37. Madshus, I. H. (1994) The N-terminal α-helix of fragment B of diphtheria toxin promotes translocation of fragment A into the cytoplasm of eukaryotic cells. *J. Biol. Chem. 269*, 17723–17729.
38. Hayashibara, M., and London, E. (2005) Topography of diphtheria toxin A chain inserted into lipid vesicles. *Biochemistry 44*, 2183–12196.
39. Hu, V. W., and Holmes, R. K. (1984) Evidence for direct insertion of fragments A and B of diphtheria toxin into model membranes. *J. Biol. Chem. 259*, 12226–12233.
40. Wolff, C., Wattiez, R., Ruysschaert, J. M., and Cabiaux, V. (2004) Characterization of diphtheria toxin's catalytic domain interaction with lipid membranes. *Biochim. Biophys. Acta 1661*, 166–177.
41. Montecucco, C., Schiavo, G., and Tomasi, M. (1985) pH-dependence of the phospholipid interaction of diphtheria-toxin fragments. *Biochem. J. 231*, 123–128.
42. Barbieri, J. T., and Collier, R. J. (1987) Expression of a mutant, full-length form of diphtheria toxin in *Escherichia coli*. *Infect. Immun. 55*, 1647–1651.
43. Bradford, M. M. (1976) A rapid and sensitive method for the quantitation of microgram quantities of protein utilizing the principle of protein-dye binding. *Anal. Biochem. 72*, 248–254.
44. Finkelstein, A., Oh, K. J., Senzel, L., Gordon, M., Blaustein, R. O., and Collier, R. J. (2000) The diphtheria toxin channel-forming T-domain translocates its own NH2-terminal region and the catalytic domain across planar phospholipid bilayers. *Int. J. Med. Microbiol. 290*, 435–440.
45. Lakkis, F., Steele, A., Pacheco-Silva, A., Rubin-Kelley, V., Strom, T. B., and Murphy, J. R. (1991) Interleukin 4 receptor targeted cytotoxicity: Genetic construction and in vivo immunosuppressive activity of a diphtheria toxin-related murine interleukin 4 fusion protein. *Eur. J. Immunol. 21*, 2253–2258.
46. Oh, K. J., Senzel, L., Collier, R. J., and Finkelstein, A. (1999) Translocation of the catalytic domain of diphtheria toxin across planar phospholipid bilayers by its own T domain. *Proc. Natl. Acad. Sci. U.S.A. 96*, 8467–8470.
47. Blewitt, M. G., Chung, L. A., and London, E. (1985) Effect of pH on the conformation of diphtheria toxin and its implications for membrane penetration. *Biochemistry 24*, 5458–5464.
48. Zhan, H., Choe, S., Huynh, P. D., Finkelstein, A., Eisenberg, D., and Collier, R. J. (1994) Dynamic transitions of the transmembrane domain of diphtheria toxin: Disulfide trapping and fluorescence proximity studies. *Biochemistry 33*, 11254–11263.
49. Sharpe, J. C., Kachel, K., and London, E. (1999) The effects of inhibitors upon pore formation by diphtheria toxin and diphtheria toxin T domain. *J. Membr. Biol. 171*, 223–233.
50. Sharpe, J. C., and London, E. (1999) Diphtheria toxin forms pores of different sizes depending on its concentration in membranes: Probable relationship to oligomerization. *J. Membr. Biol. 171*, 209–221.
51. Tortorella, D., Sesardic, D., Dawes, C. S., and London, E. (1995) Immunochemical analysis shows all three domains of diphtheria

toxin penetrate across model membranes. *J. Biol. Chem. 270*, 27446–27452.
52. Zhao, G., and London, E. (2006) An amino acid "transmembrane tendency" scale that approaches the theoretical limit to accuracy for prediction of transmembrane helices: Relationship to biological hydrophobicity. *Protein Sci. 15*, 1987–2001.
53. Van den Berg, B., Clemons, W. M., Jr., Collinson, I., Modis, Y., Hartmann, E., Harrison, S. C., and Rapoport, T. A. (2004) X-ray structure of a protein-conducting channel. *Nature 427*, 36–44.
54. Koronakis, V., Sharff, A., Koronakis, E., Luisi, B., and Hughes, C. (2000) Crystal structure of the bacterial membrane protein TolC central to multidrug efflux and protein export. *Nature 405*, 914–919.
55. Erlandson, K. J., Miller, S. B., Nam, Y., Osborne, A. R., Zimmer, J., and Rapoport, T. A. (2008) A role for the two-helix finger of the SecA ATPase in protein translocation. *Nature 455*, 984–987.
56. Zimmer, J., Nam, Y., and Rapoport, T. A. (2008) Structure of a complex of the ATPase SecA and the protein-translocation channel. *Nature 455*, 936–943.